EXPERIMENTAL INVESTIGATION OF COMPLIANT POLISHING OF FREE-FORM SUS 304 SURFACES USING THE TAGUCHI METHOD

Tran Viet Kieu[1], Nguyen Van Dai[1], Chu Ba Lam[1], Hoang Minh Duc[1], Vu Van Chung[1], Than Van Hung[2], Pham Thi Thieu Thoa[1,*]

DOI: https://doi.org/10.57001/huih5804.2026.118

ABSTRACT

This study aims to perform experimental analysis for the compliant polishing process of free-form surfaces made from SUS 304, an important material widely used in medical, construction, and various industrial fields due to its superior properties. The model integrates macro-scale analysis with micro-scale mechanisms to accurately describe the material removal mechanism, based on Hertzian contact theory. The breakthrough of this research lies in the application of an equivalent material substitution method to precisely determine the mechanical parameters of the polishing tool, a key factor previously overlooked in traditional models. The practical application in polishing SUS 304 material demonstrated superior effectiveness by achieving a surface roughness of 17nm. Additionally, this research not only provides a solution for polishing free-form SUS 304 surfaces but also establishes an important theoretical foundation for the development of advanced machining technologies in the future.

Keywords: *Compliant polishing; Material removal function; Free-form surface; Surface roughness; SUS 304.*

[1]School of Mechanical and Automotive Engineering, Hanoi University of Industry, Vietnam

[2]College of Industrial Techniques, Bac Giang, Vietnam.

[*]Email: phamthithieuthoa@haui.edu.vn

Received: 05/3/2026

Revised: 10/5/2026

Accepted: 25/5/2026

1. INTRODUCTION

SUS 304 stainless steel is extensively employed in advanced manufacturing sectors, including biomedical devices, precision molds, and functional components requiring high surface integrity, owing to its excellent corrosion resistance, mechanical strength, and biocompatibility [1-3] . Nevertheless, conventional machining processes such as milling and grinding typically introduce pronounced surface defects, including deep tool marks and subsurface damage, which necessitate subsequent polishing to meet stringent surface quality requirements [4-6]. Among the available polishing techniques, compliant polishing using a flexible polishing bonnet has emerged as a highly efficient and adaptable approach for finishing complex free-form surfaces [7, 8]. Compared with non-contact or semi-contact techniques such as ion beam polishing and magnetic polishing, bonnet-based compliant polishing offers notable advantages in terms of material removal efficiency, process flexibility, and applicability to large-area and complex geometries [9, 10]. Despite its effective application, the basic comprehension and simulation of how material is abraded during bonnet-based processes remain underdeveloped, particularly for complex metallic geometries such as those made from SUS 304.

Existing theoretical models for polishing processes have predominantly relied on the classical Preston equation or simplified Gaussian pressure distribution assumptions, which primarily describe macro-scale phenomena based on contact pressure and relative velocity[11, 12]. While these models provide useful first-order approximations, they fail to account for critical micro-scale mechanisms, including abrasive particle surface interactions, scratch formation behavior, and the influence of polishing pad morphology. As a result, their applicability to compliant polishing of free-form metallic surfaces is inherently limited [13, 14]. To overcome these shortcomings, recent efforts have moved toward multi-scale modeling frameworks that couple macro-scale contact mechanics and flow behavior with micro-scale material removal mechanisms [15]. These approaches, validated through experimental observations, have significantly advanced the theoretical foundation for

understanding polishing dynamics [16-20]. Nevertheless, systematic experimental investigations that explicitly link multi-scale mechanisms with process parameter optimization, particularly through robust statistical design methods, remain scarce [21-25].

In this context, the present study introduces a comprehensive experimental investigation of compliant polishing for free-form SUS 304 surfaces. The material removal function is examined as a coupled outcome of workpiece geometry and key process parameters, including applied pressure, tool and machine speed, abrasive particle size, slurry concentration, and polishing pad morphology. Building upon Hertzian contact theory and abrasive scratch theory, an experimental framework is established to elucidate the interaction mechanisms governing material removal. Furthermore, the Taguchi method is employed to efficiently evaluate the relative significance of process parameters and to identify optimal polishing conditions. The novelty of this work lies in the integration of multi-scale physical modeling with a statistically rigorous experimental design, providing both mechanistic insight and practical guidelines for precision finishing of complex free-form metallic surfaces.

2. COMPLIANT POLISHING METHOD

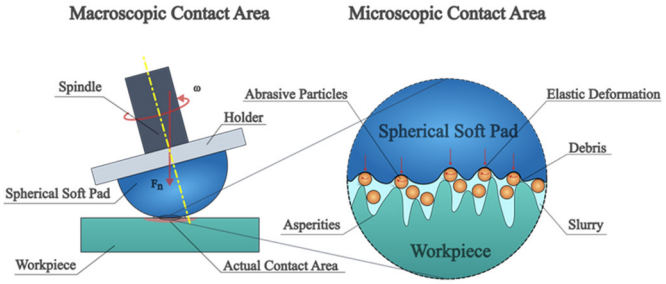

Figure 1. The millimeter-scale contact mechanics and the nano-scale abrasive interactions

The rate at which material is removed is controlled by a combination of factors, namely: the geometry of the workpiece, the normal force applied, the properties of the polishing pad, and the size of the abrasive particles (D). By contrast, the conventional Preston model accounts only for contact pressure and relative velocity at the macro scale, thereby neglecting critical micro-scale factors such as abrasive-induced scratch formation mechanisms and the physicochemical composition of the polishing fluid. As illustrated in Figure 1, while macro-scale contact behavior is characterized by millimeter-scale Interface Surfaces, the actual material removal process is dominated by micro- and nano-scale abrasive interactions, where individual particles engage the surface through micro-cutting and plowing mechanisms. To address these limitations, recent studies have developed multi-scale modeling frameworks that integrate macro-, micro-, and nano-scale models to achieve a more comprehensive understanding of the underlying interaction mechanisms governing material removal.

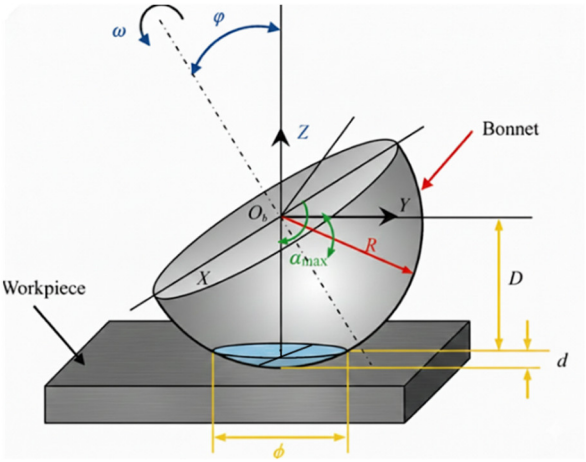

Figure 2. Schematic illustration of the polishing mechanism using a compliant polishing tool

According to kinematic theory, the relative velocity between the polishing pad and the target surface in the polishing zone can be expressed as:

$$V(x,y,S,\varphi,R_b,d)=\frac{\pi S}{30}.\sqrt{\begin{matrix}(y\cot\varphi-(R_b-d))^2.(\sin\varphi)^2\\+x^2(\cos\varphi)^2\end{matrix}} \quad (1)$$

where, $x^2+y^2\le(R_b)^2-(R_b-d)^2$, S is the angular speed in rpm, φ is the tilt angle, d is the polishing depth in mm, R_b is the radius of the polishing bonnet in mm. Because the plasticity index of the compliant polishing pad is approximately one order of magnitude lower than that of the metallic workpiece, the pad–workpiece interaction is predominantly elastic, except in cases involving extremely rough surfaces. In addition, the material removal capability of an abrasive particle is strongly governed by its geometric morphology. Angular particles generate higher material removal rates than spherical ones due to their enhanced cutting and plowing actions; consequently, abrasives with conical or angular shapes are commonly employed in polishing processes. As schematically illustrated in Figure 2, the compliant polishing mechanism involves elastic deformation of the pad that enables abrasive particles to engage the workpiece surface in a controlled manner. For the sake of theoretical tractability, the contact among the pad, workpiece, and abrasive particles is modeled as a

solid-solid interaction, while the influence of fluid flow is neglected and the particle size is assumed to remain constant. For processes utilizing flexible polishing layers and sparse grit distribution , the density of participating abrasive media is generally a function of the effective tool footprint as well as the volumetric fraction of the slurry, which aligns with established observations.

2.1. An Analysis of Interface Pressure Across Compliant Polishing Tools and Workpieces at the Macro Scale

Mathematical Model for Determining Interface Surface

The spatial configuration of the mass abrasion zone is established through the contact footprint where the compliant head engages with the component. The flexible polishing head assembly features a three-layer construction: an inner metal backing, an intermediate silicone buffer, and an outer compliant pad. The pad thickness is significant, being comparable to the bonnet's radius (within one order of magnitude), and therefore must be incorporated into the analysis. As a result, the functional radius of the finishing apparatus is determined by adding the core radius of the spherical component R_{bonnet} to the depth of the outer compliant layer t_{pad}.

$$R = R_{bonnet} + t_{pad} \tag{2}$$

Interaction between the tool and the machined surface induces a polishing force F and a defined contact area S. This interface establishes the contact patch geometry, playing a crucial role in the distribution of material removal. The applied pressure is primarily derived from the strain energy stored within the compliant strata of the tool. According to Hertzian contact theory, for a given tool displacement d, this force can be expressed as:

$$F = \frac{4}{3}\sqrt{ER}\sqrt{d^3} \tag{3}$$

In this formulation, E represents the elastic modulus of the polishing tool and d is the prescribed vertical displacement (tool deviation). Determining the Interface Surface for complex curvatures requires the concurrent consideration of both the tool and workpiece geometries. As established by elasticity theory, the contact interface between a spherical bonnet tool and a curved workpiece forms an elliptical region, commonly designated as the tool's functional processing footprint (Figure 1). The composite curvature radius R^* which encapsulates the combined influence of both contacting surfaces, is the key parameter defining these contact characteristics.

$$\frac{1}{R^*} = \frac{1}{R} - \frac{1}{R_{gauss}} \tag{4}$$

R_{gauss} represents the local radius of curvature of the target surface. Considering the major radius a and semi-minor axis b of the resulting elliptical contact region, their dimensions are derived from Equations (5) and (6). Subsequently, the total Interface Surface S is computed using Equation (7):

$$a = \lambda_1 \sqrt[3]{\left(\frac{3FR^*}{4E^*}\right)} \tag{5}$$

$$b = \lambda_2 \sqrt[3]{\left(\frac{3FR^*}{4E^*}\right)} \tag{6}$$

$$S = \pi ab = \pi\lambda_1\lambda_2 \sqrt[3]{\left(\frac{3FR^*}{4E^*}\right)^2} \tag{7}$$

In Formula (7), λ_1 and λ_2 represent variables derived from the geometric curvature relationship characterizing the tool-substrate interface, as defined in the literature. For the specific curvature conditions in this study, these coefficients take the values, $\lambda_1 = 1.1$ and $\lambda_2 = 0.9$. Equation (7) demonstrates that the Interface Surface at any specific point is governed exclusively by the local curvature of the substrate, meaning it remains invariant with respect to the global reference system. Furthermore, E^* denotes the composite modulus of elasticity describing the interaction of the contacting pair, which is derived from their material characteristics as defined by Equation (8):

$$\frac{1}{E^*} = \frac{1-v_w^2}{E_w} + \frac{1-v_b^2}{E_b} \tag{8}$$

Here, E_w represent the Young's modulus (168GPa) and Poisson coefficient (0.3) of the single-crystal silicon layer, respectively, while v_b denotes the Poisson parameter of the flexible finishing head. The effective modulus of elasticity E^* calculated from these material properties, serves as the fundamental parameter governing the Interface Surface.

2.2. The Removal Mechanism of an Individual Abrasive Particle within the Contact Zone

The process of stock removal is primarily dictated by the microscopic engagement of polishing grains with the target substrate located inside the working interface. Consequently, investigating the dynamics of an individual cutting grain is essential. The contact pressure transmitted through the compliant tool loads these particles, enabling them to indent and remove material via micro-cutting and

plowing (Figure 1). The approximate Interface Surface connecting the compliant layer and a discrete abrasive sphere is $1/4\pi D^2$. Thus, the normal force F_N acting on one particle can be estimated as:

$$F_N = \frac{1}{4}\pi D^2 P_{(x,y,z)} \quad (9)$$

In Equation (9), D represents the mean abrasive particle diameter. Material removal during polishing is governed by two principal mechanisms: plastic deformation or brittle fracture. Because of the minute grit dimensions and dense spatial arrangement, the force sustained by individual grains usually remains below the threshold needed to initiate fractures. As a result, in standard finishing scenarios, rigid grits mainly induce ductile deformation on the target substrate, establishing plastic flow as the principal mechanism of mass subtraction within the bonnet finishing process. Based on Hertzian contact mechanics, the contact radius σa at the junction of a loaded abrasive grain and the machined face is defined by the equation:

$$\sigma_a = \sqrt[3]{\left(\frac{3F_N D}{8E_w^*}\right)} \quad (10)$$

In equation (10), E^* is determined from the elastic properties of both materials using the relation:

$$\frac{1}{E_w^*} = \frac{1-v_w^2}{E_w} + \frac{1-v_g^2}{E_g} \quad (11)$$

E_g and v_g denote the the elastic stiffness and transverse strain ratio of the abrasive media. In this research, Al_2O_3 particles are selected, exhibiting a modulus of elasticity of 87GPa and a Poisson constant of approximately 0.17. The indentation depth h_w produced by a particle relates to its mechanical contact radius σa through the following kinematic relationship:

$$\sigma_a^2 = \left(\frac{D}{2}\right)^2 - \left(\frac{D}{2} - h_w\right)^2 = h_w(D - h_w) \approx Dh_w \quad (12)$$

Subsequently, by substituting Equation (10) into Equation (12), the abrasive penetration depth h_w is derived as:

$$h_w = \frac{1}{D}\sqrt[3]{\left(\frac{3F_N D}{8E_w^*}\right)^2} \quad (13)$$

Bonnet polishing relies on plastic flow as the dominant removal mechanism. Thus, the abrasive penetration depth(h_w) must satisfy $h_w > h_{elastic}$, where $h_{elastic}$ is the minimum depth required to achieve plastic deformation rather than elastic rebound. This critical depth is given by:

$$h_{elastic} = \frac{11.98\pi^2(1-v_w)^4 H_w^2}{32c^2 E_w^2} D \quad (14)$$

Here c denotes the contact coefficient, which is typically assigned a value of 3. The onset of plastic flow deformation is conventionally assumed to occur when the contact pressure surpasses a threshold of approximately 0.4Hw. Where Hw represents the workpiece hardness parameter. The minimum penetration to induce ductile yielding is consistently smaller than the critical value needed to propagate brittle fracture $h_{plastic}$ as defined below:

$$h_{plastic} = \frac{9cF_N^3(1-v_w^2)^2}{32\pi k^* \sigma_a^3 E_w^2} D \quad (15)$$

In this expression, k^* denotes a coefficient for pressure calibration, strictly bounded by the interval (0, 1). From Equations (13), (14), and (15), the effective cutting depth is constrained to the following interval:

$$h_{elastic} < h_w < h_{plastic} \quad (16)$$

The onset of material removal is marked by the progression from reversible elasticity to permanent deformation, which occurs when the cutting depth goes beyond the material's yield point. Regarding an individual abrasive grain, the instantaneous removal rate is derived from the cross-sectional area of its generated groove, ΔS (calculated from the contact diameter and indentation depth), multiplied by the particle's instantaneous velocity.

$$\Delta S = 2\sigma_a h_w \quad (17)$$

$$\Delta V = 2\sigma_a h_w v_{(x,y,z)} \quad (18)$$

3. EXPERIMENTAL SETUP AND DISCUSSION

3.1. Experimental Setup/Configuration

All empirical investigations were executed via a polishing machine system integrated with a robotic arm (Figure 3). The system uses a 3-layer polishing bonnet (metal, silicon, soft pad), with the advantage that the silicon layer absorbs vibration and provides flexibility when working on complex surfaces, while remaining stable under long-term or high-speed working conditions. The Interface Surface is flexibly adjusted through tool pressure and tool deviation. The 6-axis Doosan robot, with integrated force/torque sensors, enables precise force control, ensuring uniform polishing surface quality.

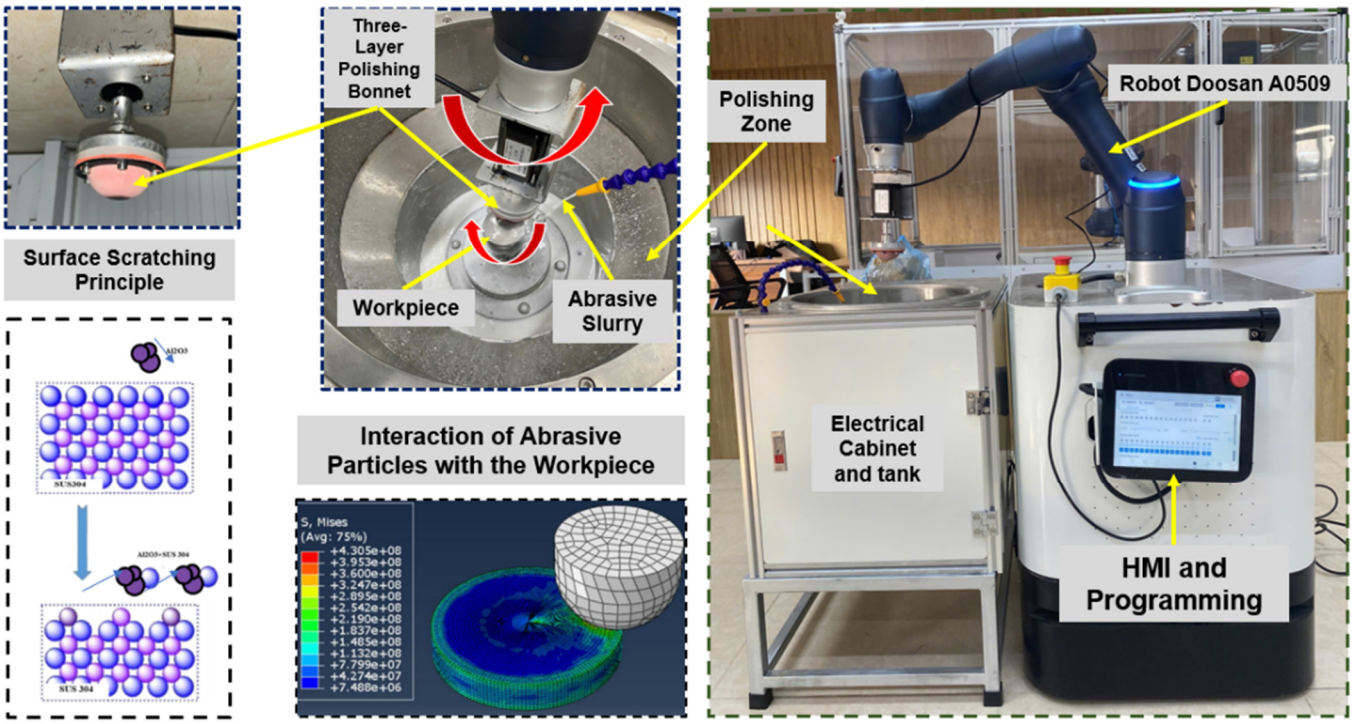

Figure 3. Polishing experimental setup

The target face (anterior) is designed with an off-axis parabolic topology, whereas the supporting rear face forms a cylindrical geometry with a 200mm radius. The primary objective is to finish the anterior side, which possesses a curvature radius of 3.491013mm and a decentration (offset) of 200mm. The mathematical representation of this profile is expressed in Formula (19):

$$\begin{Bmatrix} z^2 + x^2 = 6.982026y \\ 5694 \le y \le 5764 \\ -45 \le x \le 45 \end{Bmatrix} \quad (19)$$

3.2. ANOVA Analysis Results for the Compliant polishing Process

Table 1. Experimental parameters for polishing

Level	$V_{machine}$	V_{tool}	Abrasive Slurry Mix Ratio (%)		
			Al_2O_3	Coolant Oil	Deionized Water
1	225	115	10	5	85
2	300	140	10	10	80
3	350	150	15	10	75

The Taguchi experimental design method is widely employed to systematically investigate the influence of multiple input parameters and their respective levels on process output responses. Owing to its efficiency, this approach has been successfully applied across diverse engineering fields to reduce experimental time and cost while identifying optimal parameter combinations. In the present study, the polishing parameters and their corresponding levels selected for the Taguchi design are summarized in Table 1, which provides a structured overview of the experimental factors considered in the polishing process.

The Taguchi method selected the optimal solution based on Analysis of Variance (ANOVA) and the Signal-to-Noise ratio (S/N ratio). The degree of influence of factors on output parameters is evaluated through the S/N ratio. This index is defined by the formula:

$$(S/N)_i = 10\log\left[\frac{\overline{y_i}^2}{s_i^2}\right] \quad (20)$$

where $\overline{y_i} = \frac{1}{N}\sum_{u=1}^{N_i} y_{i,u}$ is the signal, $s_i^2 = \frac{1}{1-N}\sum_{u=1}^{N_i}\left(y_{i,u} - \overline{y_i}\right)^2$ is the noise, i is the experiment number, u is the sequence number, and Ni is the number of measurements. The S/N ratio value is large (large signal, small noise) when this output parameter is close to the optimal value. In a minimization problem (smaller is better), formula (20) is expressed as:

$$(S/N)_i = -10\log\left[\sum_{u=1}^{N_i}\frac{y_i^2}{N_i}\right] \quad (21)$$

In a maximization problem (larger is better), Formula (20) is written as:

$$(S/N)_i = -10\log\left[\frac{1}{N_i}\sum_{u=1}^{N_i}\frac{1}{y_u^2}\right] \quad (22)$$

Table 2. Roughness measurement results under different technological conditions

Level	$V_{machine}$	V_{tool}	Abrasive Slurry	Ra (µm)
1	1	1	1	0.072
2	1	2	2	0.094
3	1	3	3	0.042
4	2	1	2	0.068
5	2	2	3	0.089
6	2	3	1	0.051
7	3	1	3	0.029
8	3	2	1	0.020
9	3	3	2	0.017

Factor	Average S/N ratio		
	V machine	*V tool*	*Slurry*
1	13,44	14,80	16,01
2	13,31	14,15	16,01
3	21,38	16,75	16,11
Mean	16,04	15,23	16,04
Maximum	13,31	14,15	16,01
Optimization	221 (*V machine level 2; V tool level 2; slurry level 1*)		

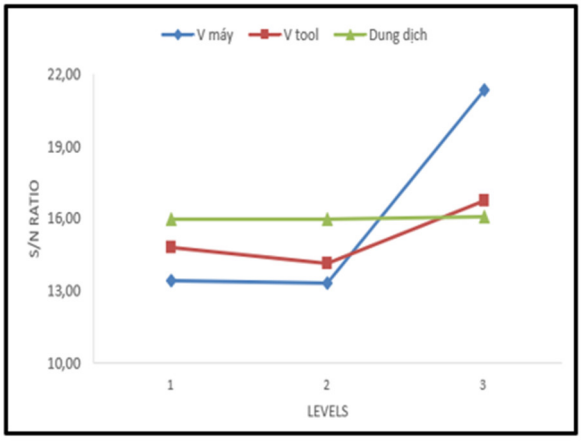

Figure 4. ANOVA analysis results

The ANOVA results obtained from the polishing experiments are presented in Figure 4. The analysis indicates that the machine speed (V_machine) exhibits the lowest signal-to-noise (S/N) ratio of 13.31 at level 2, identifying it as the most influential factor affecting surface roughness. This is followed by the tool speed (V_tool), which shows an S/N ratio of 14.15 at level 2. In contrast, the slurry concentration demonstrates a comparatively higher minimum S/N ratio of 16.01 at level 1, suggesting a less pronounced influence on surface roughness. Consistent with the roughness measurement results summarized in Table 2, the abrasive slurry mixing ratio is observed to have a negligible effect on surface roughness within the investigated parameter range. Based on the ANOVA results, the optimal polishing condition corresponds to case 221, defined by V_machine = 300, V_tool = 140, and a slurry composition of 10%, 5%, and 85%, respectively.

3.3. Interface Surface Estimation

The Interface Surface directly establishes the boundaries of the tool-engagement area on the machined surface. To validate the calculation model presented in Section 2.1.1 (Equation 7), a series of measurements were performed on the experimental setup (Figure 5). The model predicts that the Interface Surface is a function of the local geometric curvature specific to the contact interface's center. Experiments were conducted by incrementally increasing the tool displacement d in steps of 0.1 mm at a constant speed, with five repetitions per step to ensure statistical reliability. The results confirm that the tool's effective elastic modulus varies with applied load, and a proportional relationship between the theoretical Interface Surface and tool displacement was observed, consistent with the model's predictions.

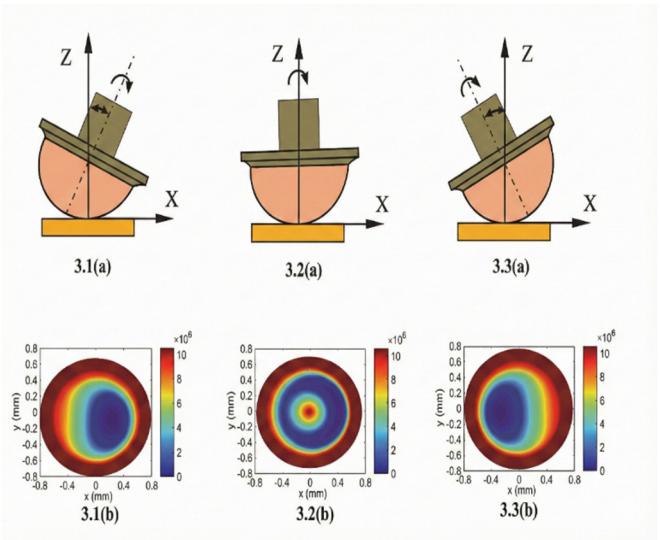

Figure 5. Interface Surface corresponding to the three stages of deviation

3.4. Spot Polishing Experimental Investigation

To validate the accuracy of the material removal model, a series of fixed-point polishing experiments were conducted, followed by simulation. This section presents the actual morphology and cross-sectional profile of the polished spots obtained experimentally. The peak attainable depth of material erosion for every experimental configuration was analyzed, providing critical data for determining the depth of cut required to eliminate the subsurface damaged layer in subsequent polishing operations. Figure 6 shows the measured material morphology obtained from these experiments.

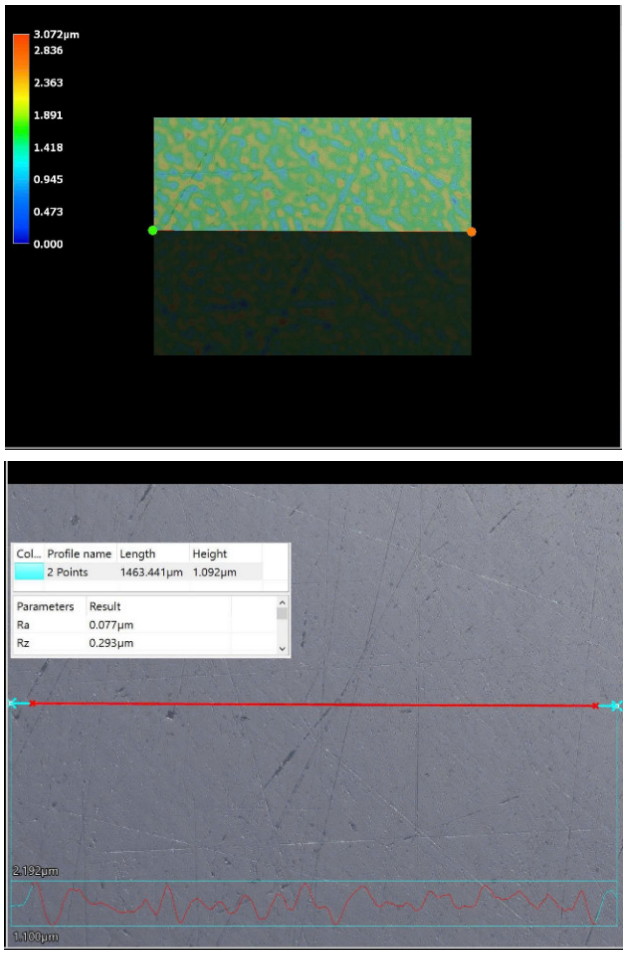

Figure 6. Material morphology measured by machine

3.5. Practical Polishing Experiment

Figure 7 presents the quantitative and qualitative surface morphology measurements obtained using the VHX-7000 digital microscope (KEYENCE, VHX series), providing a detailed comparison of the workpiece surface conditions before and after polishing. The measurement results reveal pronounced differences in surface topography, highlighting the effectiveness of the proposed polishing process. Prior to polishing, the surface exhibits a highly irregular morphology characterized by deep, randomly distributed scratches and prominent asperities, which are indicative of severe mechanical damage introduced during the preceding machining stages. As illustrated in Figure 8, which compares the spherical workpiece surface before and after polishing, the initially rough surface is progressively transformed into a significantly smoother topography. Following polishing, the original deep grooves are largely eliminated and replaced by much finer and shallower scratches with a more uniform distribution. This transition reflects a shift in the dominant material removal mechanism from aggressive micro-cutting to controlled micro-scale abrasion and smoothing.

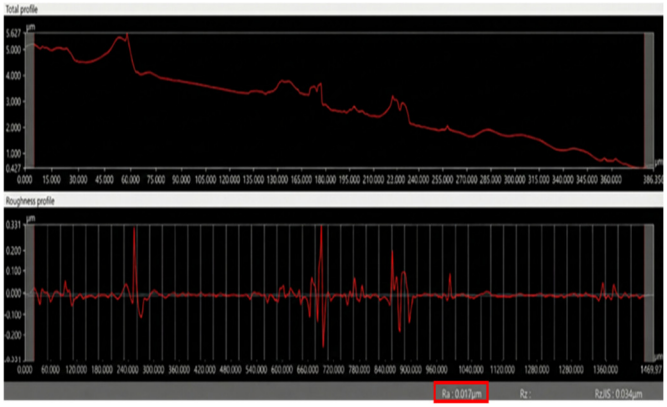

Figure 7. Measurement results

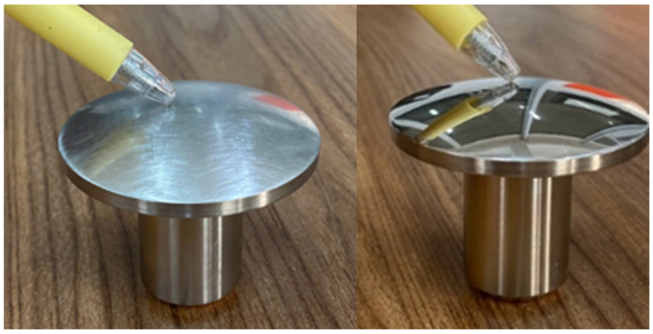

Figure 8. Spherical workpiece surface before and after polishing

Moreover, the post-polishing surface exhibits a marked reduction in surface roughness, with the formation of a surface texture approaching the nanometer scale. The Figure 7 confirm that the height variation across the polished surface is substantially diminished, resulting in a more homogeneous and continuous surface morphology. Such improvements are particularly critical for spherical components, where surface integrity directly influences functional performance, including contact behavior and wear resistance. Overall, the comparative observations from Figures 7 and 8 demonstrate that the proposed polishing

strategy effectively suppresses deep surface defects while promoting the generation of a high-quality nanometer-scale surface. These results validate the capability of the polishing process to achieve superior surface finishing on complex spherical workpieces, thereby confirming its potential applicability in high-precision engineering and SUS 304 surface manufacturing.

4. CONCLUSION

This study successfully establishes a multi-factor, optimized ratio modeling framework for simulating and analyzing the polishing behavior of free-form surfaces fabricated from SUS 304 stainless steel. By systematically integrating macro-scale contact mechanics including contact dynamics, pressure distribution, and relative velocity fields with micro-scale material removal mechanisms such as abrasive particle surface interactions and scratch formation governed by Hertzian contact theory, the proposed model effectively addresses the inherent limitations of the conventional Preston approach, which considers only pressure and velocity at the macro level. Beyond theoretical advancement, the model demonstrates strong practical relevance by enabling an intelligent overlapping path polishing strategy that ensures uniform material removal across complex free-form geometries. Experimental validation confirms that the optimized parameter combinations derived from the model lead to a significant enhancement in surface quality, achieving a final surface roughness as low as 17nm. This level of surface finish highlights the model's robustness and reliability in capturing the coupled multi-scale interactions that govern polishing performance. Overall, the proposed framework provides a comprehensive and scalable approach for precision surface finishing, offering valuable insights into process optimization for complex geometries. The findings not only extend the theoretical understanding of compliant polishing mechanisms but also present a practical pathway for improving surface integrity in high-precision manufacturing applications, thereby underscoring the potential of the proposed model for broader industrial implementation.

REFERENCES

[1]. Y. Xu, et al., "A short review of medical-grade stainless steel: Corrosion resistance and novel techniques," *Journal of Materials Research and Technology*, 29, 2788-2798, 2024.

[2]. A. Thakur, A. Kumar, S. Kaya, R. Marzouki, F. Zhang, L. J. C. Guo, "Recent advancements in surface modification, characterization and functionalization for enhancing the biocompatibility and corrosion resistance of biomedical implants," *Coatings,* 12, 10, 1459, 2022.

[3]. B. Thangaraj, S. N. TS Nellaiappan, R. Kulandaivelu, M. H. Lee, T. Nishimura, "A facile method to modify the characteristics and corrosion behavior of 304 stainless steel by surface nanostructuring toward biomedical applications," *ACS Applied Materials & Interfaces,* 7, 32, 17731-17747, 2015.

[4]. Z.W. Zhong, "Advanced polishing, grinding and finishing processes for various manufacturing applications: a review," *Materials and Manufacturing Processes*, 35, 12, 1279-1303, 2020.

[5]. W. Grzesik, B. Kruszynski, A. Ruszaj, "Surface integrity of machined surfaces," in *Surface integrity in machining*: Springer, 143-179, 2010.

[6]. D. De Oliveira, et al., "Abrasive and non-conventional post-processing techniques to improve surface finish of additively manufactured metals: A review," *Progress in Additive Manufacturing*, 8, 2, 223-240, 2023.

[7]. H. Feng, L. Huang, P. Huang, J. Liu, X. He, Y. Peng, "Review on high efficiency and high precision compliant polishing method," *Int J Adv Manuf Technol,* 132, 5, 2091-2128, 2024.

[8]. Z. Wu, J. Shen, Y. Peng, X. Wu, "Review on ultra-precision bonnet polishing technology," *Int J Adv Manuf Technol,* 121, 5, 2901-2921, 2022.

[9]. Y. Han, et al., "Material removal characteristics in submerged pulsating air jet polishing process," *International Journal of Mechanical Sciences,* 257, 108534, 2023.

[10]. A. Malakizadi, D. Mallipeddi, S. Dadbakhsh, R. M'Saoubi, P. Krajnik, "Post-processing of additively manufactured metallic alloys - A review," *International Journal of Machine Tools and Manufacture,* 179, 103908, 2022.

[11]. Z.C. Cao, C. Cheung, "Multi-scale modeling and simulation of material removal characteristics in computer-controlled bonnet polishing," *International Journal of Mechanical Sciences*, 106, 147-156, 2016.

[12]. J. Chaves-Jacob, A. Beaucamp, W. Zhu, D. Kono, J. Linares, "Towards an understanding of surface finishing with compliant tools using a fast and accurate simulation method," *International Journal of Machine Tools and Manufacture,* 163, 103704, 2021.

[13]. L. Nagdeve, V. Jain, J. Ramkumar, "Nanofinishing of freeform/sculptured surfaces: state-of-the-art," *Manufacturing Review*, 5, 6, 2018.

[14]. S. Kumar, Z. Tong, X. Jiang, "Advances in the design and manufacturing of novel freeform optics," *International Journal of Extreme Manufacturing*, 4, 3, 032004, 2022.

[15]. E. Van Der Giessen, et al., "Roadmap on multiscale materials modeling," *Modelling and Simulation in Materials Science and Engineering*, 28, 4, 043001, 2020.

[16]. Z. Zhong, "Recent advances in polishing of advanced materials," *Materials and Manufacturing Processes*, 23, 5, 449-456, 2008.

[17]. G. Zhao, et al., "Review on modeling and application of chemical mechanical polishing," *Nanotechnology Reviews*, 9, 1, 182-189, 2020.

[18]. M. Vadali, C. Ma, N. A. Duffie, X. Li, F. Pfefferkorn, "Pulsed laser micro polishing: Surface prediction model," *Journal of Manufacturing Processes*, 14, 3, 307-315, 2012.

[19]. J. Zhang, H. Wang, A. S. Kumar, M. Jin, "Experimental and theoretical study of internal finishing by a novel magnetically driven polishing tool," *International Journal of Machine Tools and Manufacture*, 153, 103552, 2020.

[20]. G. Yang, B. Wang, K. Tawfiq, H. Wei, S. Zhou, G. Chen, "Electropolishing of surfaces: Theory and applications," *Surface Engineering*, 33, 2, 149-166, 2017.

[21]. J. Li, J. Zhang, W. Ge, X. Liu, "Multi-scale methodology for complex systems," *Chemical Engineering Science*, 59, 8-9, 1687-1700, 2004.

[22]. Y. Liu, G. Zheng, N. Letov, Y. Zhao, "A survey of modeling and optimization methods for multi-scale heterogeneous lattice structures," *J. Mech. Des.*, 143, 4, 040803, 2021.

[23]. B. Liu, W. Lu, "Surrogate models in machine learning for computational stochastic multi-scale modelling in composite materials design," *International Journal of Hydromechatronics*, 5, 4, 336-365, 2022.

[24]. Y. Bai, H. Wang, M. Xia, F. Ke, "Statistical mesomechanics of solid, linking coupled multiple space and time scales," *Applied Mechanics Reviews*, 58, 372-388, 2005.

[25]. G. C. Peng, et al., "Multiscale modeling meets machine learning: What can we learn?," *Arch Computat Methods Eng,* 28, 3, 1017, 2020.